The Cryosphere Discuss., 8, 4033–4074, 2014
www.the-cryosphere-discuss.net/8/4033/2014/
doi:10.5194/tcd-8-4033-2014

The Cryosphere Discussions
Open Access

Warming permafrost and active layer variability at Cime Bianche, Western Alps

P. Pogliotti[1], M. Guglielmin[2], E. Cremonese[1], U. Morra di Cella[1], G. Filippa[1], C. Pellet[3], and C. Hauck[3]

[1]Environmental Protection Agency of Valle d'Aosta, Saint Christophe, Italy
[2]Dep. Theoretical and Applied Sciencies, Insubria University, Varese, Italy
[3]Department of Geosciences, University of Fribourg, Fribourg, Switzerland

Received: 17 June 2014 – Accepted: 8 July 2014 – Published: 21 July 2014

Correspondence to: P. Pogliotti (paolo.pogliotti@gmail.com)

Published by Copernicus Publications on behalf of the European Geosciences Union.

Abstract

The objective of this paper is to provide a first synthesis on the state and recent evolution of permafrost at the monitoring site of Cime Bianche (3100 m a.s.l.). The analysis is based on seven years of ground temperatures observations in two boreholes and seven surface points. The analysis aims to quantify the spatial and temporal variability of ground surface temperatures in relation to snow cover, the small scale spatial variability of the active layer thickness and the warming trends on deep permafrost temperatures.

Results show that the heterogeneity of snow cover thickness, both in space and time, is the main factor controlling ground surface temperatures and leads to a mean range of spatial variability ($2.5 \pm 0.15\,^{\circ}C$) which far exceeds the mean range of observed inter-annual variability ($1.6 \pm 0.12\,^{\circ}C$). The active layer thickness measured in two boreholes 30 m apart, shows a mean difference of 2.03 ± 0.15 m with the active layer of one borehole consistently lower. As revealed by temperature analysis and geophysical soundings, such a difference is mainly driven by the ice/water content in the sub-surface and not by the snow cover regimes. The analysis of deep temperature time series reveals that permafrost is warming. The detected linear trends are statistically significant starting from depth below 8 m, span the range 0.1–0.01 $^{\circ}C\,year^{-1}$ and decrease exponentially with depth.

Our findings are discussed in the context of the existing literature.

1 Introduction

Permafrost degradation can induce severe feedbacks on the climate system and directly on society, the first most importantly by greenhouse gas release in sedimentary lowlands (DeConto et al., 2012; Hollesen et al., 2011; Schuur et al., 2009) and the latter by hazards from changing slope stability in densely populated mountain areas (Stoffel et al., 2014; Allen and Huggel, 2013; Haeberli, 2013; Fischer et al., 2012, 2013) or

TCD
8, 4033–4074, 2014

by damaging infrastructures lying on ice-rich permafrost layers or high-mountain summits (Bommer et al., 2010; Springman and Arenson, 2008). Because of this sensitivity, permafrost has been defined as an important cryospheric indicator of global climate change (e.g., Harris and Haeberli, 2001).

The study of permafrost in mountain regions has become relevant in view of ongoing climate changes (Etzelmüller, 2013; Harris et al., 2009; Gruber and Haeberli, 2007; Gruber, 2004). Although permafrost warming and increasing active layer thickness has been observed worldwide (Harris, 2003; Smith et al., 2010; Romanovsky et al., 2010; Wu and Zhang, 2008; Christiansen et al., 2010; Guglielmin and Cannone, 2012; Guglielmin et al., 2014a), in mountain areas the complex topography, the ground surface type, the snow cover, the subsurface hydrology and geology strongly influence the thermal regime of mountain permafrost (Gruber and Haeberli, 2009) altering the response to changing environmental conditions.

In the Alps a number of permafrost monitoring sites exists (e.g., Cremonese et al., 2011). At present the long-term observation of temperatures in boreholes provides the best direct evidence of permafrost state and evolution. Moreover the combination of geophysical and thermal monitoring approaches, such as electrical resistivity tomography (ERT) and boreholes temperature, have been shown to be particularly suitable for permafrost long-term monitoring (e.g., Hilbich et al., 2008; Haeberli et al., 2010; PERMOS, 2013).

The long-term monitoring of ground surface temperature and related spatial variability on differing types of land covers is also crucial because of its direct implications on the initialization, calibration and validation of numerical models (e.g., Guglielmin et al., 2003; Noetzli and Gruber, 2009; Hipp et al., 2014). Snow cover exerts an important influence on the ground thermal regime based on differing processes (Zhang, 2005; Luetschg et al., 2008; Guglielmin et al., 2014b). In mountain environment, on gently inclined slopes, it mostly causes a net increase of mean annual ground temperature due to its insulating effect during winter, but timing and thickness of first snow cover, the mean snow cover thickness as well as the timing of melt-out strongly control the local

TCD
8, 4033–4074, 2014

magnitude of this effect (Hoelzle et al., 2003; Brenning et al., 2005; Pogliotti, 2010). In addition to the snow cover also the characteristics of the ground surface (e.g. bedrock, debris, grain size) have a major influence on both near-surface and sub-surface temperatures as well as on downward heat propagation (Gruber and Hoelzle, 2007; Gubler et al., 2011; Rödder and Kneisel, 2012; Schneider et al., 2012).

The active layer of mountain permafrost is of particular interest because of its influence on slope processes (e.g., Fischer et al., 2012) and infrastructure stability (e.g., Bommer et al., 2010). Active layer development is mainly controlled by air temperature, solar radiation, topography, ground surface characteristics, water content and by the timing, distribution and physical characteristics of the snow cover (Zhang, 2005; Luetschg et al., 2008; Scherler et al., 2010; Wollschläger et al., 2010; Zenklusen Mutter and Phillips, 2012). As a consequence it displays both high spatial and temporal variability (Anisimov et al., 2002; Wright et al., 2009). In the Swiss Alps, the thickness of the active layer typically varies between 0.5 and 8 m depth (Gruber and Haeberli, 2009; PERMOS, 2009, 2013). Compared to the deeper thermal regime, which reacts to long-term changes in climate the active layer responds more to short-term variations like seasonal snow and air temperature conditions (Beltrami, 2002).

The permafrost temperature regime (at depths of 10 to 200 m) is a sensitive indicator of the decade-to-century climatic variability and long-term changes in the surface energy balance. This is because the range of inter-annual temperature variations decrease significantly with depth, while decadal and longer time-scale variations penetrate to greater depths into permafrost with less attenuation. As a result the signal-to-noise ratio (i.e. long term variation vs. inter-annual variability) increases rapidly with depth and the ground acts as a natural low-pass filter of the climate signal (Romanovsky et al., 2002). However, due to the rough topography and its influence on subsurface thermal regime, the geothermal profiles in mountain permafrost are disturbed and their interpretation can be problematic (Gruber et al., 2004). In addition, most of the Alpine permafrost temperature series cover time periods shorter than 20 years since the longest borehole temperature series in the Alps started in the Murtèl–Corvatsch

TCD
8, 4033–4074, 2014

rock glacier in the late 1980s (Harris, 2003). Therefore appropriate statistical models to analyze trends of decadal or even shorter time series are needed in order to extract the maximum information from such short time series (Bence, 1995; Helsel and Hirsch, 1992). Although these time series do not yet allow long-term trend analyses, they allow first assessments on the thermal state of the permafrost and its development over the past decade (Zenklusen Mutter et al., 2010).

Within this context, the monitoring site of Cime Bianche, on the Italian side of the Western Alps, has been designed for the long-term monitoring of permafrost and ground surface temperatures. The objective of this paper is to provide a first synthesis on the state and recent evolution of permafrost related variables, focusing on: (i) the spatial and temporal variability of ground surface temperatures in relation to snow cover, (ii) the small scale (20–40 m) spatial variability of the active layer thickness and (iii) the warming trend of deep permafrost temperatures.

2 Data and methods

2.1 Site description

The Cime Bianche monitoring site (CB) is located in the western Alps at the head of the Valtournenche Valley (Valle d'Aosta, Italia, 45°55′ N–7°41′ E) on the Italian side of the Matterhorn, at 3100 m a.s.l. (Fig. 1). The site is located on a small plateau slightly westward degrading characterized by terraccettes, convexities and depressions that result in a high spatial variability of snow cover thickness during winter.

The bedrock lithology is homogeneous, mainly consisting of garnetiferous micaschists and calcschists belonging to the upper part of the Zermatt–Saas ophiolite complex (Dal Piaz, 1992). The bedrock surface is highly weathered and fractured, locally resulting in a cover of coarse-debris deposits with a thickness ranging from few centimeters to a couple of meters. The presence of small landforms like gelifluction lobes (between 0.6 to almost 5 m in length) and sorted polygons of fine material (with diame-

TCD
8, 4033–4074, 2014

ters ranging between 0.6 to 3.4 m) suggests the potential presence of permafrost and cryotic phenomena.

The climate of the area is slightly continental. The long-term mean annual precipitation is reported to be about 1000 mm year^{-1} for the period 1931–1996 (Mercalli and Cat Berro, 2003) while the in-situ records show a mean of 1200 mm year^{-1} for the period 2010–2013. The mean annual air temperature (MAAT) is about −3.2 °C (mean 1951–2011). Mean monthly air temperatures are positive from June to September while February and July are respectively the coldest and the warmest months. The site is very windy and mainly influenced by NE–NW air masses. The wind action strongly contributes to the high spatial variability of snow cover thickness.

Permafrost research in the area started in the late 1990s (Guglielmin and Vannuzzo, 1995) with repeated campaigns of BTS (Bottom Temperature of Snow) measures and glaciological observations showing that the monitoring site was probably ice-covered during the climax of the Little Ice Age. In 2003, as a preliminary investigations for site selection, the potential permafrost occurrence in the area was assessed using results from BTS, VES (Vertical Electrical Soundings) and ERT (Electrical Resistivity Tomography) and the application of numerical models like Permakart (Keller, 1992) and Permaclim (Guglielmin et al., 2003). Results of this preliminary analysis (unpublished) revealed that the area is characterized by the presence of discontinuous permafrost.

2.2 Instrumentation

The site instrumentation started in 2005 and has been progressively upgraded during the following years. The current setting is nearly unchanged since August 2008 and consists of: two boreholes, a spatial grid of ground surface temperatures measures and one automatic weather station.

TCD
8, 4033–4074, 2014

2.2.1 Boreholes

A deep (DP) and a shallow (SH) borehole, reaching a depth of 41 and 6 m respectively, located about 30 m apart (Fig. 1), have been drilled in 2004 with core-destruction method. Both boreholes are 127 mm in diameter with a 60 mm sealed PVC pipe for sensor housing. The boreholes are equipped with thermistor chains based on resistors type YSI 44031 (resolution 0.01 °C, absolute accuracy ±0.05 °C and relative accuracy ±0.02 °C). Sensors depths in meters from the surface are 0.02, 0.3, 0.6, 1, 1.6, 2, 2.3, 2.6, 3, 3.3, 3.6, 4, 4.6, 5.9 for SH and 0.02, 0.3, 0.6, 1, 1.6, 2, 2.6, 3, 3.6, 4, 6, 8, 10, 12, 14, 15, 16, 17, 18, 20, 25, 30, 35, 40, 41 for DP. In each borehole, the shallower sensors (0.02 and 0.3 m) are cabled on two independent chains and are used to measure the ground surface temperature (GST) outside the PVC tube in order to avoid the thermal disturbance of the casing. Temperatures are sampled every 10 min and recorded by a Campbell Scientific CR800 datalogger. The system is equipped with a GPRS module for daily remote data transmission.

2.2.2 Ground surface temperature grid (GSTgrid)

A small grid (40 m × 10 m) is used for monitoring the spatial variability of GST (Ground Surface Temperature). The grid consists of 5 nodes, 4 at the corners and 1 in the center (Fig. 1). Each node is equipped with 2 platinum resistors PT1000 (resolution 0.01 °C, accuracy ±0.05 °C) buried in the ground at depths of 0.02 and 0.3 m (according to Guglielmin, 2006). Ground temperatures are recorded hourly by a Geoprecision D-Log12 datalogger.

For the analysis, also the GST measured at the two boreholes are included, thus 7 nodes are overall considered. Ground surface at each node is mainly characterized by coarse-debris with a fine matrix of coarse-sand and fine-gravel. At each node, the sensors are placed in the matrix thus local ground conditions are nearly homogeneous between all nodes. In contrast, snow cover conditions sharply differ across the grid nodes. Based on field observations and temperature time series analysis (Schmid et al., 2012)

TCD
8, 4033–4074, 2014

the set is divided in *snow-free* and *snow-covered* nodes. The first group includes 3 nodes characterized by shallow or intermittent winter snow cover while the latter group includes 4 nodes that clearly show a long lasting deep snow cover with a damping of temperature oscillations during winter (Fig. 1).

2.2.3 Automatic weather station

An automatic weather station (AWS) is installed just above the borehole SH since 2006. Air temperature and relative humidity, atmospheric pressure, wind speed and direction, incoming and outgoing short- and long-wave solar radiation and snow depth are recorded every 10 min by a Campbell Scientific CR3000 datalogger. The system is equipped with a GPRS module for the daily remote data transmission. Since September 2011 a second snow depth sensor has been installed in the surroundings of the DP borehole. Finally solid and liquid precipitations are measured since January 2009 by an OTT Pluvio^2 system.

2.3 Data analysis

This section reports a short description of the criteria applied for the calculation of the synthesis parameters used in this study.

MAGT is the mean annual ground temperature at a specific depth (m) (e.g. $MAGT_{10}$).

MAGST is the mean annual ground surface temperature. It is calculated with the sensors at 0.02 m or 0.3 m of depth (specified each time).

ALT is the active layer thickness defined as the maximum depth (m) reached by the 0 °C isotherm at the end of the warm season. It is calculated considering the maximum daily temperature at each sensor depth and interpolating between the deepest sensor with positive value and the sensor beneath. The maximum of the resulting vector and the corresponding day are named ALT and ALTday respectively. Such procedure is applied on the warmest period (in depth) of the year, here fixed from 1 August to 30 November.

TCD
8, 4033–4074, 2014

TTOP is the MAGT at the top of the permafrost table (Smith and Riseborough, 1996). It is calculated by interpolation of the MAGT at depth of the ALT that is considering the first sensors just above and the first just below the ALT.

THO is the thermal offset within the active layer and is computed as TTOP-MAGST (Burn and Smith, 1988).

ZAA is the depth beneath which there is almost no annual fluctuation in ground temperature, nominally smaller than 0.1 °C (van Everdingen, 2005). The annual fluctuation (AF) is calculated at each sensor depth as the difference between annual maximum and annual minimum of the mean daily temperatures. The ZAA is calculated by interpolation between the deepest sensor with AF greater than 0.1 °C and the sensor beneath. On deep nodes time series (below 8 m), a moving average window of 360 days is applied on hourly data before the daily aggregation to remove the electrical sensor's noise (sometimes present).

All the synthesis parameters listed above, with the exception of ALT, are computed considering as reference period the hydrological year (beginning 1 October). All the analysis are performed with the free statistical software R (R Core Team, 2014). When appropriate, the variability of the results is expressed in terms of standard error (se = $\mathrm{sd}/\sqrt{n}$ where se is standard error, sd is standard deviation and n is the sample size).

2.4 Trend analysis

In order to look for linear trends that might reflect warming, two non-parametric methods are applied to boreholes temperatures: Mann–Kendall test (MK) (Mann, 1945; Kendall, 1948) and Sen's slope estimator (SS) (Sen, 1968). These methods are commonly used to assess trends and related significance levels in hydro-meteorological time series such as water quality, stream flow, temperature and precipitation (e.g., Gocic and Trajkovic, 2013; Kousari et al., 2013). The reason for using non-parametric statistical tests is that they are more suitable for non-normally distributed data and are not sensitive to outliers or abrupt changes.

TCD
8, 4033–4074, 2014

The procedure chosen includes (i) a pre-whiten of the data for removing the lag-1 autocorrelation components as recommended by von Storch and Navarra (1999) (see also Hamed, 2009), (ii) fitting of the trend's slope with SS and (iii) testing of trend's significance level (p value) with MK. Such a procedure is implemented in the R-package zyp (Bronaugh et al., 2013).

Given the short climatological time-span of the given borehole's observations, a seasonal detrending is recommended, as suggested by Helsel and Hirsch (1992), for better discerning the long-term linear trend over time. Thus a seasonal decomposition based on loess smoother (Cleveland, 1979; Cleveland et al., 1990) is applied on the monthly aggregated time series of each borehole before applying SS and MK (Fig. 2). Such a seasonal detrending method is implemented by the R-function *stl* (R Core Team, 2014).

2.5 Geophysics

At the end of the summer 2013, two geophysical surveys took place at the Cime Bianche with the objective to assess the composition of the subsurface. A first explorative geoelectric (ERT) profile was performed on 16 August 2013, and on 9 October 2013 the ERT measurement was repeated in combination with one refraction seismic tomography (RST) along the same line (see Fig. 1). Combining refraction seismic and ERT measurements enables to unambiguously identify the subsurface materials in the ground. Due to very different specific resistivities, ERT is best suited to differentiate between ice and water whereas the distinction between air and ice can more easily be accomplished by RST, because of large contrasts between their respective p wave velocities.

2.5.1 Electrical Resistivity Tomography (ERT)

A 94 m long electrode array composed of 48 electrodes with 2 m spacing was installed along a straight line less than two meters far from the two boreholes (Fig. 1). Current

TCD
8, 4033–4074, 2014

was injected using varying electrode pairs, and the resulting potential differences were automatically measured by a Syscal (Iris Instruments) for each quadrupole possible with the Wenner–Schlumberger configuration (529 measurements, 23 depth levels). The electrode locations were marked with spray paint and a number of electrodes were left on site to facilitate further measurements.

The measured apparent resistivity datasets were then inverted using the RES2DINV software (Geotomosoft, 2014) with the following set-up. A robust inversion constraint was applied to avoid unrealistic smoothing of the calculated specific resistivities. Additionally the depth of the model layers was increased by a factor 1.5 and an extended model was used to match the model grid of the corresponding seismic inversion. Note, that for geometric reasons, the two lower corners of the resulting tomograms have very low sensitivity to the obtained data and should not be over-interpreted. Finally, a time-lapse inversion scheme was applied to the two ERT data sets yielding the percentage of resistivity change from the first measurements to the second. Here, an unconstraint inversion was chosen, meaning that the ERT measurements were inverted independently.

2.5.2 Refraction Seismic Tomography (RST)

The measurements were conducted using a Geode seismometer (Geometrics) and 24 geophones placed with 4 m spacing. A seismic signal was generated in-between every second geophone pair by repeatedly hitting a steel plate with a sledge hammer. To improve the signal-to-noise ratio the signal was stacked at least 15 times at each location. Two additional offset shot points were measured (3 m before the first geophone and 6 m beyond the last one) in order to maximize the spatial resolution and match the ERT profile length and depth of investigation.

The first arrivals of the seismic *p* wave were manually picked for each seismogram using the software REFLEXW (Sandmeier, 2014). A Simultaneous Iterative Reconstruction Technique (SIRT) algorithm was then used to reconstruct a 2-D tomogram of *p* wave velocity distribution based on the obtained travel times. Starting from a syn-

TCD
8, 4033–4074, 2014

thetic model the travel times are calculated and compared to the measured ones. The model is then updated iteratively by minimizing the residuals between measured and calculated travel times.

3 Results

3.1 Ground surface temperatures

Figure 3 shows MAGST at 2 and 30 cm of depth for each hydrological year calculated on the seven GST nodes. The analysis of the GST dataset shows a mean range of the spatial variability of 2.5 ± 0.15 °C versus a mean range of the inter-annual variability of 1.6 ± 0.12 °C. Some years (e.g. 2009, 2011, 2013) show a MAGST spatial variability that can be greater than 3 °C, far exceeding the observed mean inter-annual variability.

The time series analysis of snow-covered nodes (Schmid et al., 2012) reveals that the mean duration of the insulating snow cover is about 270 days while on snow-free nodes such effect is only sporadic or absent (not shown). On average the thermal offset due to snow cover is about 1.5 ± 0.17 °C with snow covered nodes usually warmer than snow-free nodes. These observations confirm that the warming and cooling effects of respectively a thick and thin snow cover (Zhang, 2005; Pogliotti, 2010) can coexist over short distances (< 50 m) and lead to high spatial variability of the GST.

The results are similar at both depth. The difference between MAGST measured at 2 cm and 30 cm is, on average, 0.4 ± 0.11 °C with deeper sensors usually warmer than the shallower ones.

3.2 Active layer

Table 1 summarizes the active layer variables observed in the two boreholes. Since August 2008 data are available at both SH and DP boreholes hence results of ALT can be compared over 6 years while MAGST, TTOP and THO over 5 years (shaded rows

TCD
8, 4033–4074, 2014

in Table 1). Missing values (column %NA) in both boreholes are lower than 4 % in all years.

ALT is the variable showing the greater difference between the two boreholes with a mean of 2.75 ± 0.35 m in SH and 4.78 ± 0.26 m in DP. The mean inter-annual difference of ALT between the two boreholes is 2.03 ± 0.12 m while the mean absolute inter-annual variability of ALT at borehole level is 1 ± 0.13 m. In both boreholes the maximum ALT has been recorded in 2012 while the minimum in 2010. ALT-Day is normally anticipated in DP (except 2013) with differences ranging from few days (e.g. 2009) to more than 3 weeks (e.g. 2012). The MAGST is on average slightly lower in SH which normally shows a thinner winter snow cover compared to DP (Fig. 4). The TTOP values are very similar, around −0.9 °C. The THO is negative in both boreholes (except 2013) with a mean value of about −0.5 °C in DP and −0.3 °C in SH.

The values of Table 1 show that all the active layer variables are very similar between the two boreholes with the only exception of ALT which in DP is nearly double than in SH. To better understand the causes of this difference, the daily mean temperatures at selected depths within the active layer of both boreholes and the corresponding snow cover thickness are compared in Fig. 4. Despite a consistently thinner snow depth is recorded on SH compared to DP (mean difference ∼ 41 ± 14 cm during the winter seasons 2012 and 2013), the duration of the insulating snow cover is similar (250 ± 16 days for SH vs. 254 ± 17 days for DP) and effectively does not determine a big difference in MAGST (Table 1). Consequently the snow cover regimes above the two boreholes can be considered equivalent and snow probably plays a major role for the inter-annual variability of ALT while the observed spatial differences must be explained otherwise.

For these reasons we hypothesize that ALT difference may be related to a greater ice/water content in SH compared to DP. This is also revealed by the geophysical survey (see Sect. 3.4 and Fig. 7) and can be inferred by temperature at greater depth. At 1.6 m (red lines, Fig. 4) a pronounced zero-curtain effect can be observed in SH (dashed lines) twice per year, (i) from snow melt to mid-summer and (ii) from the snow onset to mid-winter, while a similar behavior is missing in DP. The occurrence of the

TCD
8, 4033–4074, 2014

zero-curtain reflects a large consumption of energy, both for ice melting during summer and water freezing during winter resulting in lower temperatures of SH. Deeper down, the summer heat wave in SH is further delayed if compared to DP: at 3 m in SH (dashed blue lines) the zero-curtain effect is almost continuous from late-summer to early-winter (e.g. in 2010 and 2011) and it is not possible to see a breaking point between melting and freezing processes. Such a behavior is totally missing in DP. It is also interesting to observe that freezing zero-curtain ends nearly contemporary at 1.6 and 3 m and is followed by a rapid temperature drop.

In conclusion, the ALT at Cime Bianche shows a pronounced spatial variability probably caused by the variability of ice/water content in the sub-surface and associated energy consumption resulting from freezing and melting processes.

3.3 Permafrost temperature and warming trend

Due to the small depth reached by the borehole SH, the analysis of deep temperature and permafrost temperature is limited to the borehole DP. Looking at temperature profiles with depth (Fig. 5), the permafrost layer at Cime Bianche has a thickness greater than 40 m and a mean temperature of about −1.2 °C. The ZAA varies across years and during the observation period ranged from a minimum of 14.2 m in 2011 to a maximum of 16.2 m in 2013 (Table 2). During the observed years, both minimum (solid lines) and maximum (dashed lines) temperature profiles (deeper than 8 m) tend to progressively shift toward warmer temperatures (Fig. 5). The only exceptions are represented by the 2011's maximum and the 2009's minimum, the latter only above 10 m of depth.

The observed temperature shift is also quantitatively supported by the trend analysis performed on deeper sensors (range 8–41 m of depth, Fig. 6). The analysis has been conducted at all depths within both boreholes but only trends below 8 m have shown to be significant (Kendall's p value of the time series < 0.01) hence only DP borehole is shown. Figure 6 reveals that a pronounced warming rate is present at all depths although it exponentially decrease with depth, varying from around 0.1 °C year^{-1} at 8 m to 0.007 °C year^{-1} at 41 m. The upper boundaries of the confidence intervals (CI) are

TCD
8, 4033–4074, 2014

systematically unbalanced toward higher values and the lower boundaries are always above zero. This means that, at all depths, the statistical distribution of all possible fitted trends is asymmetric towards greater values and also that negative significant trend have never been fitted by the model.

Based on the trend analysis, is possible to conclude that permafrost at Cime Bianche is degrading with a warming rate decreasing with depth.

3.4 Geophysics

Figure 7 shows the final distribution of specific resistivity for the two ERT measurements, the percentage of change in the model resistivity between the two time steps and the *p* wave velocity distribution over the same subsection. Additionally, the surface characteristics and a detailed analysis of the geophysical properties at the two borehole locations (SH and DP, Fig. 8) are included in the analysis.

The overall characteristics of both ERT profiles are very similar (Fig. 7a and b) and can be divided into three main zones: a low resistive layer directly below the surface varying between 2.5 m thickness at the top of the slope to 7 m thickness at the bottom, respectively, two high resistive areas with values exceeding 20 000 Ω m located below the superficial layer (from the start of the subsection to the superficial borehole, 0–34 m and between 40–52 m) and a less high resistive area on the lower part of the profile below 5 m depth.

Comparing the two ERT data sets (cf. also the time-lapse image in Fig. 7c), one can observe a clear increase of the uppermost low resistive layer between August and October which is coherent with a thickening of the active layer observed in the borehole temperature during this period. Another main difference between the two measurements is the apparition of two low resistive zones at 34 m and 60 m visible down to 10 m and 15 m depth, respectively. These areas can also be seen in the ERT tomogram from August, but much less developed and limited to a few meters. In addition, the very high resistive area located in the upper part of the profile is much smaller and displaced of about 5 m towards the lower part of the profile in the second measurement.

TCD
8, 4033–4074, 2014

These changes are clearly visible in blue (increase) and red (decrease) colors in Fig. 7c. As said before the two datasets were inverted independently within the time-lapse scheme. A constrained inversion (results not shown here) would yield very similar overall distribution of resistivity changes the only difference being a much smaller range of values. The large area of resistivity increase located just above the superficial borehole location and reaching down to the bottom of the profile corresponds to the displacement of the high resistive area observed in the ERT tomograms.

The RST tomogram exhibits much less lateral variations than the ERT results (see Fig. 7d), pointing to the influence of liquid water in the ERT results. One can clearly see a relatively slow layer with velocities between 300 and 1500 m s^{-1} (red and dark red colors) just below the surface with varying thickness between 3 and 5 m. This layer is thickest in the vicinity of the shallow borehole (SH) and thinnest at DP (64 m). Below this first layer the velocities increase steadily until reaching the maximum (around 6400 m s^{-1}). The rate of velocity increase is strongest around 40 m and there is a clear distinction between the upper part of the profile (until 45 m) and the lower one. At depth the high velocity zone is present in the upper part and not in the lower part of the profile. Conversely the velocities at the surface are much higher in the lower part (especially around DP) than in the upper part.

Both geophysical profiles show clear differences in the subsurface properties at the boreholes locations. To relate in detail the results yielded by the geophysics and the measured temperature, the vertical distribution of specific resistivity, seismic velocity and ground temperature at SH and DP are shown in Fig. 8.

4 Discussion

4.1 Ground surface temperatures

In this study both the inter-annual and the spatial variability of MAGST within a restricted area have been analyzed and compared: the results show that, at Cime

TCD
8, 4033–4074, 2014

Bianche, the mean range of spatial variability (2.5 ± 0.15 °C) far exceeds the mean range of observed inter-annual variability (1.6 ± 0.12 °C). Given the comparatively homogeneous characteristics of the ground surface at the sensors' locations, such a variability is essentially caused by the heterogeneity of the snow cover thickness both in space (effect of wind redistribution and micro-morphology) and time (effect of variable weather conditions and precipitations).

The thermal effect of snow cover on ground surface temperature has been extensively analyzed (e.g., Goodrich, 1982; Keller and Gubler, 1993; Zhang, 2005; Luetschg et al., 2008). In recent years, with the advances of mini-loggers technology, the number of field experiments aimed at the characterization of the spatial variability of GST has grown. Recently Gubler et al. (2011) observed a spatial variability of more than 2.5 °C within a number of square homogeneous areas of 10 m × 10 m. In Norway, Isaksen et al. (2011) report that MAGST varied by 1.5–3.0 °C over distances of 30–100 m in a region characterized by mountain permafrost. Rödder and Kneisel (2012) observed ranges exceeding 4.3 °C between adjacent loggers (< 50 m), although this values include inhomogeneities of surface characteristics. Similar results were obtained by Gisnås et al. (2014) who observed a variability of the MAGST of up to 6 °C within heterogeneous areas of 0.5 km^2.

The inter-annual variability of MAGST caused by snow is also well known and documented by a number of studies (Romanovsky et al., 2003; Hoelzle et al., 2003; Karunaratne and Burn, 2004; Brenning et al., 2005; Etzelmüller, 2007; Ødegård and Isaksen, 2008; Schneider et al., 2012) but rarely has been explicitly analyzed and quantified. An exception in the Alps is represented by Hoelzle et al. (2003) who reported an inter-annual variability of ±2.7 °C measured during two seasons on 8 mini-loggers with differing surface characteristics in the Murtèl–Corvatsch area. Our results thus report a more robust quantification of the mean inter-annual GST variability (1.6 ± 0.12 °C), based on a longer time series (7 years).

The obtained results are very similar at both measurement depth. Given such a small difference and the agreement of temperature fluctuations between 2 and 30 cm, it is

TCD
8, 4033–4074, 2014

arguable that to describe the spatial variability of GST and run long-term GST observations, measures at two or more depth are not needed.

4.2 Active layer

In this study both thaw depth and temperature fluctuations within the active layer of two adjacent boreholes have been compared. Such experimental design provides direct evidence of the small-scale spatial variability of the ALT and allow to compare the effect of snow cover and ice/water content on sub-surface temperatures.

From 2009 to 2013 the ALT at Cime Bianche varied within 2 and 5.5 m with a mean inter-annual variability of 1 ± 0.13 m. These ranges of thaw depth are comparable to those recorded in other alpine sites (PERMOS, 2013) and the same is true for the observed inter-annual variability (Anisimov et al., 2002; Christiansen, 2004; Schneider et al., 2012; Smith et al., 2010).

ALT in the borehole SH is systematically lower than in DP (mean difference 2.03 ± 0.15 m) even though all the active layer parameters (MAGST, TTOP, THO see Table 1) are very similar between the two boreholes. On one side such a similarity suggests that snow cover regimes above the two boreholes are nearly equivalent thus snow probably plays a major role just for the inter-annual variability of ALT. On the other side the pronounced spatial variability of ALT is probably caused by the variability of ice/water content in the sub-surface and associated variation of energy consumption resulting from freezing and melting processes. Probably snowmelt and meltwater infiltration along preferential discontinuities (a borehole acts a discontinuity itself) is different between SH and DP. Hilbich et al. (2008) observed at Schilthorn (Swiss Alps) a similar situation between two boreholes 15 m apart, ascribing the lower ALT of one borehole to the higher moisture contents (and related freezing) caused by preferential water flow paths from the surrounding slopes. Schneider et al. (2012) analyzed the thermal regime of four adjacent boreholes drilled on differing material (coarse debris, fine debris and bedrock) at Murtèl–Corvatsch (Swiss Alps) and recognized meltwater and ice content as the main responsible for the observed ALT spatial variability.

TCD
8, 4033–4074, 2014

The different amount of available water in the active layer of the two boreholes is also reflected by the occurrence of the zero-curtain in the borehole SH and its absence in the borehole DP. In the upper part of the active layer a pronounced zero-curtain can be observed two times per year, (i) from snow melt to mid-summer (spring zero-curtain) and (ii) from the snow onset to mid-winter (autumn zero-curtain). Recently Zenklusen Mutter and Phillips (2012) deeply analyzed similar behaviors on a sample of 10 boreholes in Switzerland observing that, on average, the duration of the spring zero-curtain is usually shorter than the autumn one and is strongly dependent on snow depth at the end of the winter. At Cime Bianche, in the deeper part of the active layer such a distinction between spring and autumn zero-curtain is not always possible. As observed also by Rist and Phillips (2005) it may happen that, below a certain depth, the ground temperature does not become positive because the energy from the summer heat wave is not sufficient to melt all ice before the onset of the subsequent winter season. This continuous zero-curtain is more probable when an higher amount of meltwater is available (Scherler et al., 2010; Kane et al., 2001) and can occur at differing depth from year to year strongly influencing the resulting ALT.

4.3 Permafrost temperature and warming trend

In order to look for trends that might reflect warming, two non-parametric methods have been applied to boreholes temperatures time series. The detected linear trends are statistically significant (Kendall's p value < 0.01) only at depth below 8 m and span the range 0.1–0.01 $^{\circ}$C year^{-1} decreasing exponentially with depth. The latter evidence suggests that at Cime Bianche the permafrost is warming from surface.

As discussed also by Zenklusen Mutter et al. (2010), the detection of trends on time series covering a short time-span needs caution and adoption of specific criteria. Moreover the estimation of uncertainties and significance levels are also fundamental to facilitate the comparisons of trends between differing sites and for reproducing trend's detection methods on others datasets.

TCD
8, 4033–4074, 2014

Permafrost warming trends have been observed worldwide, both at high latitudes (Harris, 2003; Osterkamp, 2005; Smith et al., 2005; Osterkamp, 2007; Isaksen et al., 2007; Farbrot et al., 2013; Jonsell et al., 2013) and at lower latitudes in high mountain (Vonder Mühll, 2001; Harris, 2003; Gruber, 2004; Wu and Zhang, 2008; Phillips and Mutter, 2009; Zenklusen Mutter et al., 2010; PERMOS, 2013; Haeberli, 2013).

Recently in the Alps Zenklusen Mutter et al. (2010) detected linear trends applying generalized least-square methods on daily temperature time series of two boreholes in the Muot da Barba Peider ridge (Eastern Swiss Alps). For the deep frozen bedrock between 8 and 17.5 m a general warming trend was found, with significant (p value < 0.05) values ranging respectively from 0.042 to 0.025 °C year^{-1}. At Cime Bianche a similar range of warming rate exists between 16 and 20 m. The substantial difference between the two sites is that the Swiss boreholes are drilled at the top of a NW-oriented ridge with a mean slope of 38° thus with a strong 3-D thermal effect induced by topography (Noetzli et al., 2007). In the mountains of Scandinavia Isaksen et al. (2007) reports linear warming trends between 20 and 60 m of depth ranging from about 0.05 to 0.005 °C year^{-1} respectively over three sites while Isaksen et al. (2011) found an increase in mean ground temperature between 6 and 9 m of depth at two sites, with rates ranging from about 0.015 to 0.095 °C year^{-1}. Recently at Tarfala mountain station (Sweden) Jonsell et al. (2013) found linear trends over 11 years (2001–2011) ranging from 0.047 to 0.002 °C year^{-1} between 20 and 100 m of depth respectively.

The absolute values of warming rates are difficult to compare because of differing site characteristics, differing geographical regions and differing methods used for trend's detection. Nevertheless, some similitudes exist between our and the above mentioned case studies: (i) trends are difficult to detect at shallower depth because of the higher seasonal variability of temperatures (ii) warming trends are mainly significant below 8–10 m of depth, (iii) warming trends exponentially decrease with depth, (iv) there is no evidence of negative (cooling) trends at any depth in recent literature.

TCD
8, 4033–4074, 2014

4.4 Geophysics

Given the relatively high resistivity and *P* wave velocities along the profiles, the presence of permafrost observed in the borehole data is confirmed by the geophysics over the whole profile length (Fig. 7). Moreover a clear discrepancy between the upper part of the profile, where SH is located, and the lower one with borehole DP can be seen in both, the ERT and the RST data.

At DP the *P* wave velocities indicates the presence of weathered bedrock close to the surface whereas at SH a layer of coarse-debris deposits in the uppermost 5 m is confirmed by very low *P* wave velocities. Conversely, *P* wave velocities at depth are higher for SH ($\sim 6000\,\mathrm{m\,s^{-1}}$) than for DP ($\sim 5000\,\mathrm{m\,s^{-1}}$, see also Fig. 8). This difference, also seen in the resistivity data (around 17 000 Ω m at SH and 13 000 Ω m at DP), would indicate that a larger ice content is present in the upslope part of the profile than in the lower part. This is in good agreement with the spatial variation of ALT highlighted in Sect. 3.2 and the zero curtain phase observed only at SH (see Fig. 4).

The low resistivity and low velocity layer near the surface, which thickness increases visibly between August and October in the ERT data, is considered to be the active layer. Figure 8 compares the vertical distribution of specific electrical resistivity, *P* wave velocity and temperature for both boreholes and dates. On the first glance, there seems to be a mismatch between resistivity and temperature regarding ALT for SH. However, in SH borehole temperatures in August show constant values at the freezing point between 1 and 3 m depth (between 2 and 4 m in October), the deeper level being the depth of the sharply increasing resistivity values. As resistivity is sensitive to the liquid water content its values will not increase significantly before most of this liquid water has been frozen, coinciding with a temperature increase to values below the freezing point (e.g., Hauck, 2002). Due to the higher water/ice content in SH, this phenomena (∼ vertical zero-curtain) is only seen in SH and not in DP.

In addition, considering the *P* wave velocities ($500\,\mathrm{m\,s^{-1}}$ at SH and $3000\,\mathrm{m\,s^{-1}}$ at DP), one can assume that the remaining discrepancies observed between geophysics

TCD
8, 4033–4074, 2014

and temperature data are due to very different surface and subsurface properties. The general description of the surface constitution (Fig. 7e) is already an indication of these differences: DP is located in-between two zones with big blocks (from pluri-decimetric to metric), whereas SH is located at the junction between medium size blocks (from pluri-centimetric to decimetric) mixed and non-mixed with soil. These differences in subsurface material are likely to cause the strong differences in *P* wave velocities at the two borehole locations.

The two low resistive areas (34–40 m and 53–60 m) visible already in August and more pronounced on the second ERT profile in October are interpreted as preferential water flow path. Since the melt water cannot infiltrate through the two ice-rich (high resistive) bodies close by (at 20–33 and 40–52 m horizontal distance), it is forced to follow a preferential path in between. The lower infiltration area is constrained in the upper part by the ice rich zone and in the lower one by the presence of bedrock near the surface.

Finally the displacement of the high resistive area observed near SH (blue zone at depth on the time-lapse tomogram) is most likely an inversion artefact (overcompensation) due to the appearance of the low resistive area in the second ERT profile.

5 Conclusions

This paper presents a first synthesis on the thermal state and recent evolution of permafrost in the monitoring site of Cime Bianche. The analysis has been focused on: the spatial and temporal variability of MAGST, the small scale (20–40 m) spatial variability of ALT and the warming rate of deep permafrost temperatures.

The analysis of MAGST has been conducted considering seven years of monitoring on 7 sensors located in nearly homogeneous conditions in terms of both topographic and ground surface characteristics. Such experimental design allowed to quantify the thermal effect essentially due to the snow cover variability alone. Results show that: (i) the sensors characterized by shallow or intermittent winter snow cover are sys-

TCD
8, 4033–4074, 2014

tematically colder than those with a long lasting deep snow cover; (ii) the snow cover variability alone can leads to a spatial variability of MAGST greater than its inter-annual variability.

The analysis of ALT spatial variability has been conducted within two adjacent boreholes considering 6 years of observations as well as by the analysis of ERT and seismic profiles. The results show that ALT at Cime Bianche has a pronounced spatial variability caused by a different ice/water content in the sub-surface while the snow cover probably plays a role just in the inter-annual variability of ALT.

The warming rates of ground temperatures time series below 8 m of depth have been analyzed by two non-parametric methods considering 5 years of monthly data. The results show that permafrost at Cime Bianche is degrading with a warming rate which is higher at 8 m depth and exponentially decreasing with depth. Detected trends are similar to those observed recently in others boreholes both in the Alps and northern mountain environments. Moreover a review of the existing literature reveals a number of similitudes between our findings and the existing studies.

The Supplement related to this article is available online at doi:10.5194/tcd-8-4033-2014-supplement.

Acknowledgements. The authors are grateful to the lifts company Cervino S.p.a for their continuous logistical support to the research activities at the site of Cime Bianche.

C. Pellet and C. Hauck gratefully acknowledge a grant from the Swiss National Science Foundation (project SOMOMOUNT No. 200021_143325).

References

Allen, S. K. and Huggel, C.: Extremely warm temperatures as a potential cause of recent high mountain rockfall, Global Planet. Change, 107, 59–69, doi:10.1016/j.gloplacha.2013.04.007, 2013. 4034

TCD
8, 4033–4074, 2014

Anisimov, O., Shiklomanov, N., and Nelson, F.: Variability of seasonal thaw depth in permafrost regions: a stochastic modeling approach, Ecol. Model., 153, 217–227, doi:10.1016/S0304-3800(02)00016-9, 2002. 4036, 4050
Beltrami, H.: Climate from borehole data: Energy fluxes and temperatures since 1500, Geophys. Res. Lett., 29, 2111, doi:10.1029/2002GL015702, 2002. 4036
Bence, J. R.: Analysis of short time series: correcting for autocorrelation, Ecology, 76, 628–639, 1995. 4037
Bommer, C., Phillips, M., and Arenson, L. U.: Practical recommendations for planning, constructing and maintaining infrastructure in mountain Permafrost, Permafrost Periglac., 21, 97–104, doi:10.1002/ppp.679, 2010. 4035, 4036
Brenning, A., Gruber, S., and Hoelzle, M.: Sampling and statistical analyses of BTS measurements, Permafrost Periglac., 16, 383–393, doi:10.1002/ppp.541, 2005. 4036, 4049
Bronaugh, D., Werner, A., and For the Pacific Climate Impacts Consortium: zyp: Zhang + Yue-Pilon trends package, available at: http://cran.r-project.org/package=zyp (last access: July 2014), 2013. 4042
Burn, C. and Smith, C.: Observations of the "Thermal Offset" in near-surface mean annual ground temperatures at several sites near Mayo, Yukon Territory, Canada, Arctic, 41, 99–104, doi:10.14430/arctic1700, 1988. 4041
Christiansen, H. H.: Meteorological control on interannual spatial and temporal variations in snow cover and ground thawing in two northeast Greenlandic Circumpolar-Active-Layer-Monitoring(CALM) sites, Permafrost Periglac., 15, 155–169, doi:10.1002/ppp.489, 2004. 4050
Christiansen, H. H., Etzelmüller, B., Isaksen, K., Juliussen, H., Farbrot, H., Humlum, O., Johansson, M., Ingeman-Nielsen, T., Kristensen, L., Hjort, J., and Others, A.: The thermal state of permafrost in the nordic area during the international polar year 2007–2009, Permafrost Periglac., 21, 156–181, doi:10.1002/ppp.687, 2010. 4035
Cleveland, R., Cleveland, W., McRae, J. E., and Terpenning, I.: STL: A seasonal-trend decomposition procedure based on loess, Journal of Official Statistics, 6, 3–73, 1990. 4042
Cleveland, W.: Robust locally weighted regression and smoothing scatterplots, J. Am. Stat. Assoc., 74, 829–836, doi:10.1080/01621459.1979.10481038, 1979. 4042
Cremonese, E., Gruber, S., Phillips, M., Pogliotti, P., Boeckli, L., Noetzli, J., Suter, C., Bodin, X., Crepaz, A., Kellerer-Pirklbauer, A., Lang, K., Letey, S., Mair, V., Morra di Cella, U., Ravanel, L., Scapozza, C., Seppi, R., and Zischg, A.: Brief Communication: "An inventory of

TCD
8, 4033–4074, 2014

permafrost evidence for the European Alps", The Cryosphere, 5, 651–657, doi:10.5194/tc-5-651-2011, 2011. 4035
Dal Piaz, G. V.: Le Alpi dal M. Bianco al Lago Maggiore: 13 Itinerari Automobilistici e 97 Escursioni a Piedi, Vol. 1, Seven Hills Books, Padova, Italy, 1992. 4037
DeConto, R. M., Galeotti, S., Pagani, M., Tracy, D., Schaefer, K., Zhang, T., Pollard, D., and Beerling, D. J.: Past extreme warming events linked to massive carbon release from thawing permafrost, Nature, 484, 87–91, doi:10.1038/nature10929, 2012. 4034
Etzelmüller, B.: The regional distribution of mountain permafrost in Iceland, Permafrost Periglac., 199, 185–199, doi:10.1002/ppp.583, 2007. 4049
Etzelmüller, B.: Recent advances in mountain permafrost research, Permafrost Periglac., 24, 99–107, doi:10.1002/ppp.1772, 2013. 4035
Farbrot, H., Isaksen, K., Etzelmüller, B., and Gisnås, K.: Ground thermal regime and permafrost distribution under a changing climate in Northern Norway, Permafrost Periglac., 24, 20–38, doi:10.1002/ppp.1763, 2013. 4052
Fischer, L., Purves, R. S., Huggel, C., Noetzli, J., and Haeberli, W.: On the influence of topographic, geological and cryospheric factors on rock avalanches and rockfalls in high-mountain areas, Nat. Hazards Earth Syst. Sci., 12, 241–254, doi:10.5194/nhess-12-241-2012, 2012. 4034, 4036
Fischer, L., Huggel, C., Kääb, A., and Haeberli, W.: Slope failures and erosion rates on a glacierized high-mountain face under climatic changes, Earth Surf. Proc. Land., 38, 836–846, doi:10.1002/esp.3355, 2013. 4034
Geotomosoft: Res2dinv software Tutorial: 2-D and 3-D electrical imaging surveys, available at: www.geotomosoft.com (last access: July 2014), 2014. 4043
Gisnås, K., Westermann, S., Schuler, T. V., Litherland, T., Isaksen, K., Boike, J., and Etzelmüller, B.: A statistical approach to represent small-scale variability of permafrost temperatures due to snow cover, The Cryosphere Discuss., 8, 509–536, doi:10.5194/tcd-8-509-2014, 2014. 4049
Gocic, M. and Trajkovic, S.: Analysis of changes in meteorological variables using Mann–Kendall and Sen's slope estimator statistical tests in Serbia, Global Planet. Change, 100, 172–182, doi:10.1016/j.gloplacha.2012.10.014, 2013. 4041
Goodrich, L. E.: The influence of snow cover on the ground thermal regime, Can. Geotech. J., 19, 421–432, doi:10.1139/t82-047, 1982. 4049

TCD
8, 4033–4074, 2014

Gruber, S.: Permafrost thaw and destabilization of Alpine rock walls in the hot summer of 2003, Geophys. Res. Lett., 31, L13504, doi:10.1029/2004GL020051, 2004. 4035, 4052
Gruber, S. and Haeberli, W.: Permafrost in steep bedrock slopes and its temperature related destabilization following climate change, J. Geophys. Res.-Earth, 112, F02S18, doi:10.1029/2006JF000547, 2007. 4035
Gruber, S. and Haeberli, W.: Mountain permafrost, in: Permafrost Soils, 33–44, doi:10.1007/978-3-540-69371-0, Innsbruck, Austria/Springer, 2009. 4035, 4036
Gruber, S. and Hoelzle, M.: The cooling effect of coarse blocks revisited: a modeling study of a purely conductive mechanism, in: Proceedings of the 9th International Conference on Permafrost, 557–561, 29 June–3 July 2008, Fairbanks, Alaska, USA, 2008. 4036
Gruber, S., King, L., Kohl, T., Herz, T., Haeberli, W., and Hoelzle, M.: Interpretation of geothermal profiles perturbed by topography: the alpine permafrost boreholes at Stockhorn Plateau, Switzerland, Permafrost Periglac., 15, 349–357, doi:10.1002/ppp.503, 2004. 4036
Gubler, S., Fiddes, J., Keller, M., and Gruber, S.: Scale-dependent measurement and analysis of ground surface temperature variability in alpine terrain, The Cryosphere, 5, 431–443, doi:10.5194/tc-5-431-2011, 2011. 4036, 4049
Guglielmin, M.: Ground surface temperature (GST), active layer and permafrost monitoring in continental Antarctica, Permafrost Periglac., 17, 133–143, doi:10.1002/ppp.553, 2006. 4039
Guglielmin, M. and Cannone, N.: A permafrost warming in a cooling Antarctica?, Climatic Change, 111, 177–195, doi:10.1007/s10584-011-0137-2, 2012. 4035
Guglielmin, M. and Vannuzzo, C.: Studio della distribuzione del permafrost e delle relazioni con i ghiacciai della piccola età glaciale nell'alta valtournenche (Valle d'Aosta, Italia), Atti Ticinesi di Scienze della Terra, 38, 119–127, 1995. 4038
Guglielmin, M., Aldighieri, B., and Testa, B.: PERMACLIM: a model for the distribution of mountain permafrost, based on climatic observations, Geomorphology, 51, 245–257, doi:10.1016/S0169-555X(02)00221-0, 2003. 4035, 4038
Guglielmin, M., Dalle Fratte, M., and Cannone, N.: Permafrost warming and vegetation changes in continental Antarctica, Environ. Res. Lett., 9, 045 001, doi:10.1088/1748-9326/9/4/045001, 2014a. 4035
Guglielmin, M., Worland, M. R., Baio, F., and Convey, P.: Permafrost and snow monitoring at Rothera Point (Adelaide Island, Maritime Antarctica): implications for rock weathering in cryotic conditions, Geomorphology, doi:10.1016/j.geomorph.2014.03.051, 2014b. 4035

TCD
8, 4033–4074, 2014

Haeberli, W.: Mountain permafrost research frontiers and a special long-term challenge, Cold Reg. Sci. Technol., 96, 71–76, doi:10.1016/j.coldregions.2013.02.004, 2013. 4034, 4052
Haeberli, W., Noetzli, J., Arenson, L. U., Delaloye, R., Gärtner-Roer, I., Gruber, S., Isaksen, K., Kneisel, C., Krautblatter, M., and Phillips, M.: Mountain permafrost: development and challenges of a young research field, J. Glaciol., 56, 1043–1058, doi:10.3189/002214311796406121, 2010. 4035
Hamed, K.: Enhancing the effectiveness of prewhitening in trend analysis of hydrologic data, J. Hydrol., 368, 143–155, doi:10.1016/j.jhydrol.2009.01.040, 2009. 4042
Harris, C.: Warming permafrost in European mountains, Global Planet. Change, 39, 215–225, doi:10.1016/j.gloplacha.2003.04.001, 2003. 4035, 4037, 4052
Harris, C. and Haeberli, W.: Permafrost monitoring in the high mountains of Europe: the PACE project in its global context, Permafrost Periglac., 11, 3–11, doi:10.1002/ppp.377, 2001. 4035
Harris, C., Arenson, L. U., Christiansen, H. H., Etzelmüller, B., Frauenfelder, R., Gruber, S., Haeberli, W., Hauck, C., Hölzle, M., Humlum, O., Isaksen, K., Kääb, A., Kern-Lütschg, M., Lehning, M., Matsuoka, N., Murton, J., Nötzli, J., Phillips, M., Ross, N., Seppälä, M., Springman, S., and Vonder Mühll, D.: Permafrost and climate in Europe: monitoring and modelling thermal, geomorphological and geotechnical responses, Earth-Sci. Rev., 92, 117–171, doi:10.1016/j.earscirev.2008.12.002, 2009. 4035
Hauck, C.: Frozen ground monitoring using DC resistivity tomography, Geophys. Res. Lett., 29, 12-1–12-4, doi:10.1029/2002GL014995, 2002. 4053
Helsel, D. R. and Hirsch, R. M.: Trend analysis, in: Statistical Methods in Water Resources, chap. 12, Amsterdam, Holland/Elsevier, 1992. 4037, 4042
Hilbich, C., Hauck, C., Hoelzle, M., Scherler, M., Schudel, L., Völksch, I., Vonder Mühll, D., and Mäusbacher, R.: Monitoring mountain permafrost evolution using electrical resistivity tomography: a 7-year study of seasonal, annual, and long-term variations at Schilthorn, Swiss Alps, J. Geophys. Res., 113, F01S90, doi:10.1029/2007JF000799, 2008. 4035, 4050
Hipp, T., Etzelmüller, B., and Westermann, S.: Permafrost in Alpine Rock faces from Jotunheimen and Hurrungane, Southern Norway, Permafrost Periglac., 25, 1–13, doi:10.1002/ppp.1799, 2014. 4035
Hoelzle, M., Haeberli, W., and Stocker-Mittaz, C.: Miniature ground temperature data logger measurements 2000–2002 in the Murtèl-Corvatsch area, Eastern Swiss Alps, in: Proceedings of the 8th International Conference on Permafrost, 1, 7–12, available at: http://www.geo.uzh.ch/~hoelzle/hoelzleetal2003b.pdf (last access: July 2014), 2003. 4036, 4049

TCD
8, 4033–4074, 2014

Hollesen, J., Elberling, B., and Jansson, P. E.: Future active layer dynamics and carbon dioxide production from thawing permafrost layers in Northeast Greenland, Glob. Change Biol., 17, 911–926, doi:10.1111/j.1365-2486.2010.02256.x, 2011. 4034

Isaksen, K., Sollid, J. L., Holmlund, P., and Harris, C.: Recent warming of mountain permafrost in Svalbard and Scandinavia, J. Geophys. Res., 112, F02S04, doi:10.1029/2006JF000522, 2007. 4052

Isaksen, K., Ødegård, R. S., Etzelmüller, B., Hilbich, C., Hauck, C., Farbrot, H., Eiken, T., Hygen, H. O., and Hipp, T. F.: Degrading mountain permafrost in Southern Norway: spatial and temporal variability of mean ground temperatures, 1999–2009, Permafrost Periglac., 22, 361–377, doi:10.1002/ppp.728, 2011. 4049, 4052

Jonsell, U., Hock, R., and Duguay, M.: Recent air and ground temperature increases at Tarfala Research Station, Sweden, Polar Res., 1, 1–11, available at: http://www.polarresearch.net/index.php/polar/article/view/19807 (last access: July 2014), 2013. 4052

Kane, D. L., Hinkel, K. M., Goering, D. J., Hinzman, L. D., and Outcalt, S. I.: Non-conductive heat transfer associated with frozen soils, Global Planet. Change, 29, 275–292, doi:10.1016/S0921-8181(01)00095-9, 2001. 4051

Karunaratne, K. C. and Burn, C. R.: Relations between air and surface temperature in discontinuous permafrost terrain near Mayo, Yukon Territory, Can. J. Earth Sci., 1451, 1437–1451, doi:10.1139/E04-082, 2004. 4049

Keller, F.: Automated mapping of mountain permafrost using the program PERMAKART within the geographical information system ARC/INFO, Permafrost Periglac., 3, 133–138, doi:10.1002/ppp.3430030210, 1992. 4038

Keller, F. and Gubler, H. U.: Interaction between snow cover and high mountain permafrost, Murtel-Corvatsch, Swiss Alps, in: Proceedings of the Sixth International Conference on Permafrost, Beijing, vol. 1, 332–337, 21–25 July, Zurich, Switzerland 1993. 4049

Kendall, M. G.: Rank Correlation Methods, Griffin, Oxford, England, 1948. 4041

Kousari, M. R., Ahani, H., and Hendi-zadeh, R.: Temporal and spatial trend detection of maximum air temperature in Iran during 1960–2005, Global Planet. Change, 111, 97–110, doi:10.1016/j.gloplacha.2013.08.011, 2013. 4041

Luetschg, M., Lehning, M., and Haeberli, W.: A sensitivity study of factors influencing warm/thin permafrost in the Swiss Alps, J. Glaciol., 54, 696–704, doi:10.3189/002214308786570881, 2008. 4035, 4036, 4049

Mann, H. B.: Nonparametric tests against trend, Econometrics, 13, 245–259, 1945. 4041

TCD
8, 4033–4074, 2014

Mercalli, L. and Cat Berro, D.: Atlante Climatico Della Valle d'Aosta, Vol 2, SMS, Oxford, England, 2003. 4038
Noetzli, J. and Gruber, S.: Transient thermal effects in Alpine permafrost, The Cryosphere, 3, 85–99, doi:10.5194/tc-3-85-2009, 2009. 4035
Noetzli, J., Gruber, S., Kohl, T., Salzmann, N., and Haeberli, W.: Three-dimensional distribution and evolution of permafrost temperatures in idealized high-mountain topography, J. Geophys. Res., 112, F02S13, doi:10.1029/2006JF000545, 2007. 4052
Ødegård, R. and Isaksen, K.: MAGST in mountain permafrost, Dovrefjell, southern Norway, 2001–2006, in: Proceedings of the 9th International Conference on Permafrost, 1311–1315, available at: https://www.matnat.uio.no/geo/english/research/projects/cryolink/publications/NICOPoedegaardetal.pdf (last access: July 2014), 2008. 4049
Osterkamp, T. E.: The recent warming of permafrost in Alaska, Global Planet. Change, 49, 187–202, doi:10.1016/j.gloplacha.2005.09.001, 2005. 4052
Osterkamp, T. E.: Characteristics of the recent warming of permafrost in Alaska, J. Geophys. Res.-Earth, 112, doi:10.1029/2006JF000578, 2007. 4052
PERMOS: Permafrost in Switzerland 2004/2005 and 2005/2006, Glaciological Report Permafrost No. 6/7, Tech. Rep. 6, Cryospheric Commission of the Swiss Academy of Sciences, Zurich, Switzerland, 2009. 4036
PERMOS: Permafrost in Switzerland 2008/2009 and 2009/2010, Glaciological Report Permafrost No. 10/11, Tech. Rep. 10, Cryospheric Commission of the Swiss Academy of Sciences, Zurich, Switzerland, 2013. 4035, 4036, 4050, 4052
Phillips, M. and Mutter, E.: Rapid degradation of ground ice in a ventilated talus slope: flüela Pass, Swiss Alps, Permafrost Periglac., 14, 1–14, doi:10.1002/ppp.638, 2009. 4052
Pogliotti, P.: Influence of Snow Cover on MAGST over Complex Morphologies in Mountain Permafrost Regions, Ph. D. thesis, University of Turin, Turin, Italy, 2010. 4036, 4044
R Core Team: R: A Language and Environment for Statistical Computing, R Foundation for Statistical Computing, Vienna, Austria, available at: http://www.r-project.org/ (last access: July 2014), 2014. 4041, 4042
Rist, A. and Phillips, M.: First results of investigations on hydrothermal processes within the active layer above alpine permafrost in steep terrain, Norsk Geogr. Tidsskr., 59, 177–183, doi:10.1080/00291950510020574, 2005. 4051

TCD
8, 4033–4074, 2014

Rödder, T. and Kneisel, C.: Influence of snow cover and grain size on the ground thermal regime in the discontinuous permafrost zone, Swiss Alps, Geomorphology, 175–176, 176–189, doi:10.1016/j.geomorph.2012.07.008, 2012. 4036, 4049

Romanovsky, V., Burgess, M., Smith, S., Yoshikawa, K., and Brown, J.: Permafrost temperature records: indicators of climate change, EOS T. Am. Geophys. Un., 83, 589, doi:10.1029/2002EO000402, 2002. 4036

Romanovsky, V. E., Sergueev, D. O., and Osterkamp, T. E.: Temporal variations in the active layer and near-surface permafrost temperatures at the long-term observatories in northern Alaska, Month, 8, Proceedings of the 8th International Conference on Permafrost, 21–25 July, Zurich, Switzerland 2003. 4049

Romanovsky, V. E., Drozdov, D. S., Oberman, N. G., Malkova, G. V., Kholodov, A. L., Marchenko, S. S., Moskalenko, N. G., Sergeev, D. O., Ukraintseva, N. G., Abramov, A., Gilichinsky, D., and Vasiliev, A. A.: Thermal state of permafrost in Russia, Permafrost Periglac., 21, 136–155, doi:10.1002/ppp.683, 2010. 4035

Sandmeier: ReflexW Scientific Software, Sandmeier geophysical research, available at: www.sandmeier-geo.de, Karlsruhe, Germany, 2014. 4043

Scherler, M., Hauck, C., Hoelzle, M., Stähli, M., and Völksch, I.: Meltwater infiltration into the frozen active layer at an alpine permafrost site, Permafrost Periglac., 21, 325–334, doi:10.1002/ppp.694, 2010. 4036, 4051

Schmid, M.-O., Gubler, S., Fiddes, J., and Gruber, S.: Inferring snowpack ripening and melt-out from distributed measurements of near-surface ground temperatures, The Cryosphere, 6, 1127–1139, doi:10.5194/tc-6-1127-2012, 2012. 4039, 4044

Schneider, S., Hoelzle, M., and Hauck, C.: Influence of surface and subsurface heterogeneity on observed borehole temperatures at a mountain permafrost site in the Upper Engadine, Swiss Alps, The Cryosphere, 6, 517–531, doi:10.5194/tc-6-517-2012, 2012. 4036, 4049, 4050

Schuur, E. A. G., Vogel, J. G., Crummer, K. G., Lee, H., Sickman, J. O., and Osterkamp, T. E.: The effect of permafrost thaw on old carbon release and net carbon exchange from tundra, Nature, 459, 556–9, doi:10.1038/nature08031, 2009. 4034

Sen, P. K.: Estimates of the regression coefficient based on Kendall's tau, J. Am. Stat. Assoc., 63, 1379–1389, doi:10.1080/01621459.1968.10480934, 1968. 4041

TCD
8, 4033–4074, 2014

Smith, M. and Riseborough, D.: Permafrost monitoring and detection of climate change, Permafrost Periglac., 7, 301–309, doi:10.1002/(SICI)1099-1530(199610)7:4<301::AID-PPP231>3.0.CO;2-R, 1996. 4041
Smith, S. L., Burgess, M., Riseborough, D., and Mark Nixon, F.: Recent trends from Canadian permafrost thermal monitoring network sites, Permafrost Periglac., 16, 19–30, doi:10.1002/ppp.511, 2005. 4052
Smith, S. L., Romanovsky, V. E., Lewkowicz, A. G., Burn, C. R., Allard, M., Clow, G., Yoshikawa, K., and Throop, J.: Thermal state of permafrost in North America: a contribution to the international polar year, Permafrost Periglac., 21, 117–135, doi:10.1002/ppp.690, 2010. 4035, 4050
Springman, S. and Arenson, L. U.: Recent advances in permafrost geotechnics, in: Proceedings of the 9th International Conference on Permafrost, 1685–1694, 29 June–3 July 2008, Fairbanks, Alaska, USA, 2008. 4035
Stoffel, M., Tiranti, D., and Huggel, C.: Climate change impacts on mass movements – case studies from the European Alps, Sci. Total Environ., doi:10.1016/j.scitotenv.2014.02.102, 2014. 4034
van Everdingen, R. O.: Multi-language glossary of permafrost and related ground-ice terms, Tech. rep., International Permafrost Association, Boulder, Colorado, available at: https://nsidc.org/fgdc/glossary/ (last access: July 2014), 2005. 4041
von Storch, H. and Navarra, A.: Analysis of climate variability: applications of statistical techniques, Springer, Berlin, Germany, 1999. 4042
Vonder Mühll, D.: Thermal variations of mountain permafrost: an example of measurements since 1987 in the Swiss Alps, in: Global Change and Protected Areas, 83–95, Springer Netherlands, 2001. 4052
Wollschläger, U., Gerhards, H., Yu, Q., and Roth, K.: Multi-channel ground-penetrating radar to explore spatial variations in thaw depth and moisture content in the active layer of a permafrost site, The Cryosphere, 4, 269–283, doi:10.5194/tc-4-269-2010, 2010. 4036
Wright, N., Hayashi, M., and Quinton, W. L.: Spatial and temporal variations in active layer thawing and their implication on runoff generation in peat-covered permafrost terrain, Water Resour. Res., 45, W05414, doi:10.1029/2008WR006880, 2009. 4036
Wu, Q. and Zhang, T.: Recent permafrost warming on the Qinghai-Tibetan Plateau, J. Geophys. Res., 113, D13108, doi:10.1029/2007JD009539, 2008. 4035, 4052

TCD
8, 4033–4074, 2014

Zenklusen Mutter, E. and Phillips, M.: Active layer characteristics at ten borehole sites in Alpine permafrost terrain, Switzerland, Permafrost Periglac., 23, 138–151, doi:10.1002/ppp.1738, 2012. 4036, 4051

Zenklusen Mutter, E., Blanchet, J., and Phillips, M.: Analysis of ground temperature trends in Alpine permafrost using generalized least squares, J. Geophys. Res., 115, F04009, doi:10.1029/2009JF001648, 2010. 4037, 4051, 4052

Zhang, T.: Influence of the seasonal snow cover on the ground thermal regime: an overview, Rev. Geophys., 43, RG4002, doi:10.1029/2004RG000157, 2005. 4035, 4036, 4044, 4049

TCD
8, 4033–4074, 2014

Table 1. Synthesis parameters of active layers recorded in the two boreholes of Cime Bianche. Refer to Sect. 2.3 for acronyms.

H.Y.	ALT [m]		ALT [date]		MAGST [°C]		MAPT [°C]		THOFF [°C]		%NA	
	SH	DP	SH	DP	SH	DP	SH	DP	SH	DP	SH	DP
2006	3.07	–	11 Oct	–	–	–	–	–	–	–	–	–
2007	2.45	–	14 Oct	–	−0.34	–	−0.78	–	−0.44	–	0	–
2008	1.9	3.94	27 Sep	25 Sep	−2.13	–	-1.82	–	0.31	–	4.38	–
2009	3.05	4.93	24 Oct	20 Oct	−0.03	0.01	−0.68	−0.85	−0.65	−0.86	3.28	3.28
2010	1.87	3.86	18 Oct	8 Oct	−1.11	−1.16	−1.19	−1.28	−0.08	−0.12	1.37	1.37
2011	3.3	5.13	8 Nov	23 Oct	−0.47	0.13	−1.1	−1.01	−0.63	−1.14	0.27	0
2012	3.58	5.42	30 Oct	4 Oct	−0.4	−0.26	−0.79	−0.72	−0.39	−0.46	2.74	3.01
2013	1.96	4.6	13 Oct	13 Oct	−1.3	−0.67	−0.98	−0.58	0.32	0.09	3.6	3.59
Avg. 2009–2013	2.75 ± 0.35	4.78 ± 0.26	24 Oct	13 Oct	−0.66 ± 0.23	−0.39 ± 0.23	−0.94 ± 0.09	−0.88 ± 0.12	−0.28 ± 0.18	−0.49 ± 0.22	2.25 ± 0.62	2.25 ± 0.68

TCD
8, 4033–4074, 2014

Table 2. Interpolated ZAA depths and corresponding mean temperatures in the borehole DP.

H.Y.	ZAA (ΔT = 0.1 °C)	
	Depth [m]	Temp. [°C]
2009	15.56	−1.34
2010	15.24	−1.25
2011	14.22	−1.29
2012	15.38	−1.24
2013	16.28	−1.21
Avg.	15.33	−1.26

TCD
8, 4033–4074, 2014

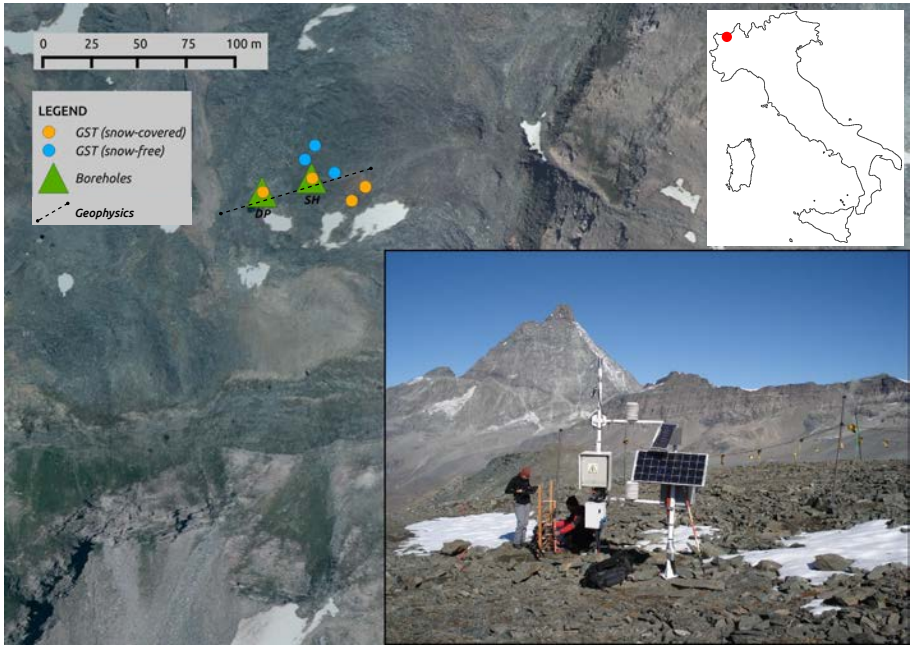

Figure 1. Overview of the Cime Bianche monitoring site.

TCD
8, 4033–4074, 2014

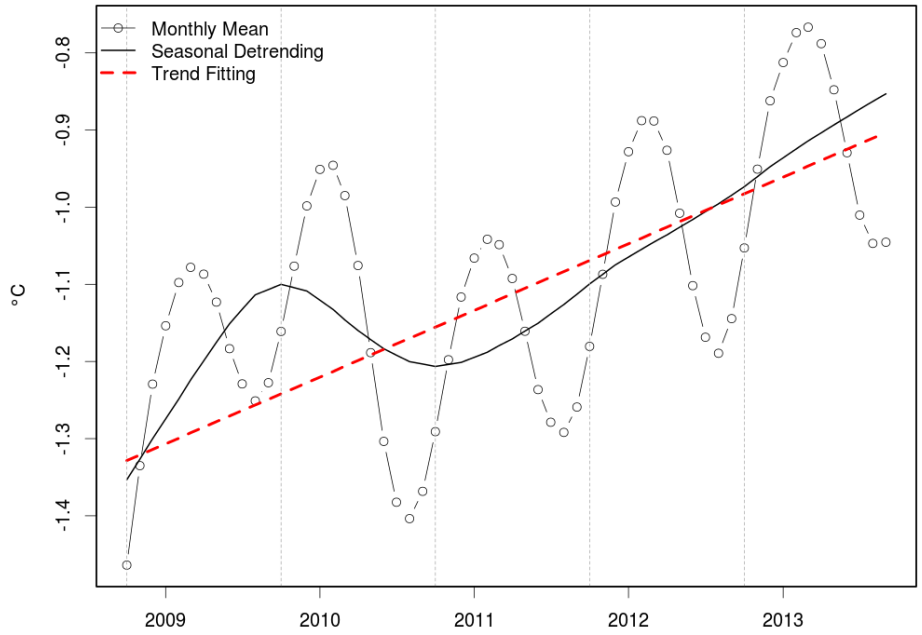

Figure 2. Methodological steps of trend analysis: (1) monthly aggregation, (2) seasonal detrending, (3) trend fitting. Vertical dashed lines represents the 1 October, materializing the limits of the hydrological years.

TCD
8, 4033–4074, 2014

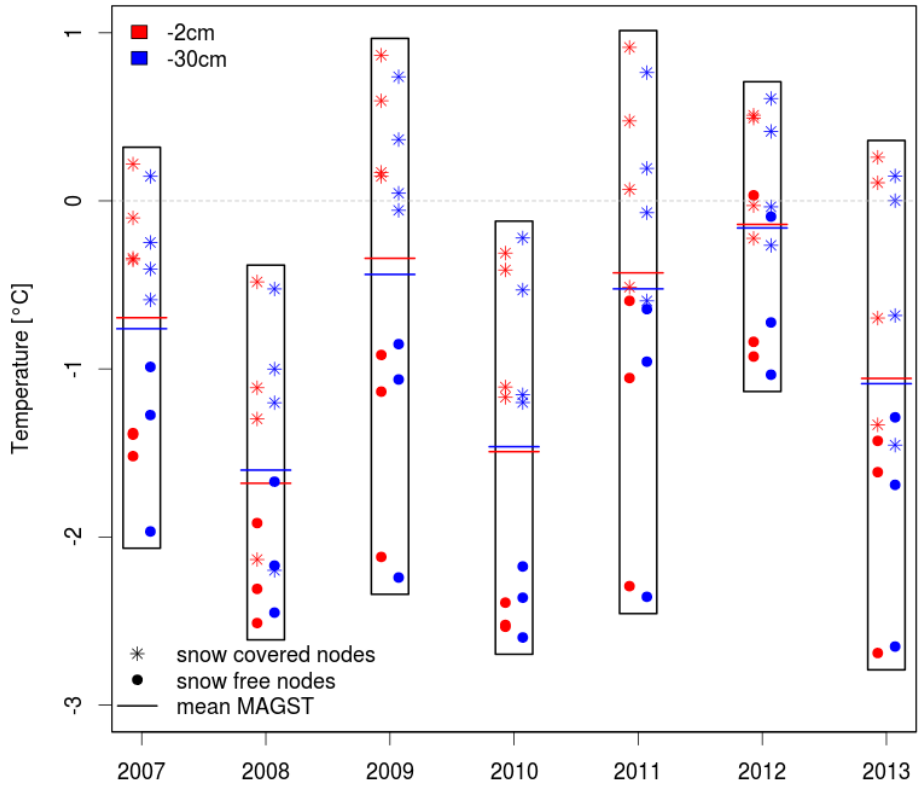

Figure 3. Mean annual ground surface temperatures at 2 cm (red) and 30 cm (blue) of depth. Star symbols indicate snow-covered nodes while bullets indicate snow-free nodes. The horizontal lines indicate the mean of all MAGST for each year and each depth. Black rectangles are used to highlight the min–max envelope for inter-annual comparison.

TCD
8, 4033–4074, 2014

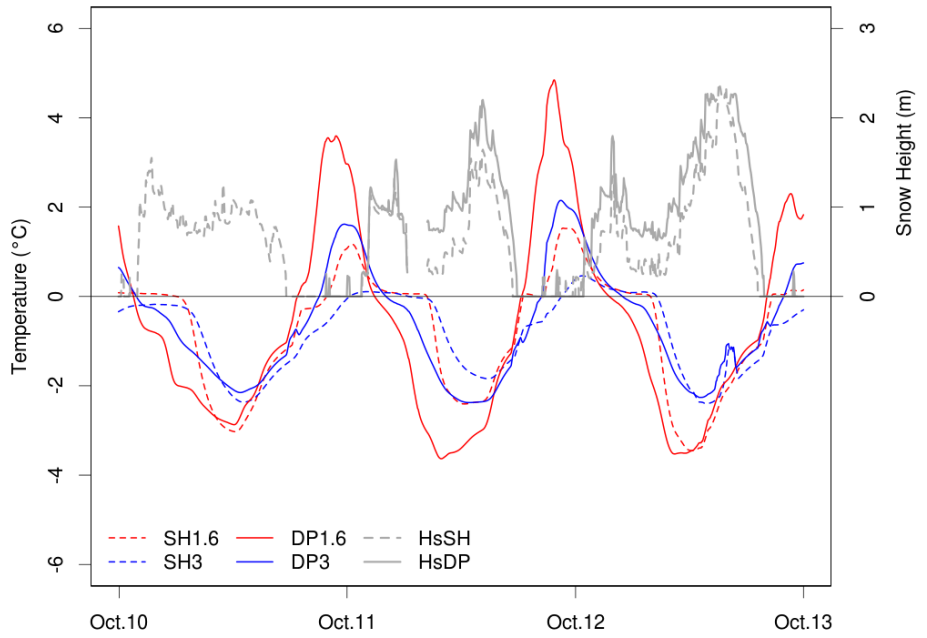

Figure 4. Fluctuations of snow cover thickness (Hs) and ground temperatures (daily mean) at selected depths in the active layers of Cime Bianche from 1 October 2010 to 30 September 2013. Lines type: dashed is for SH, solid is for DP. Colors: red is for shallower temperatures (1.6 m), blu is for deeper temperature (3 m), grey is for snow.

TCD
8, 4033–4074, 2014

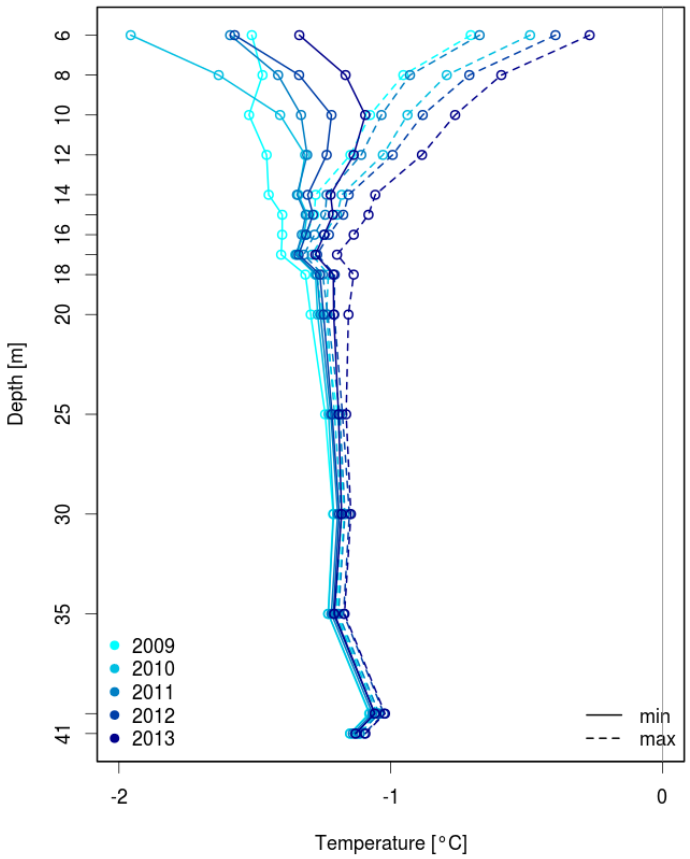

Figure 5. Minimum (solid lines) and maximum (dashed lines) temperature profiles in the borehole DP.

TCD
8, 4033–4074, 2014

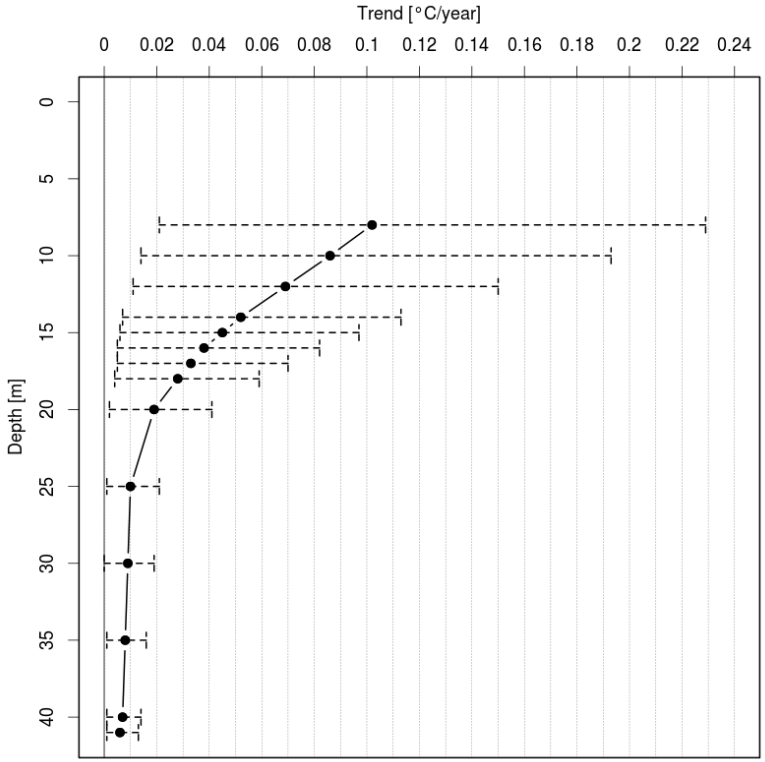

Figure 6. Warming rate below 8 m in the borehole DP as a function of depth. Black dots represent linear trends as $^{\circ}$C year^{-1}. The uncertainty of trend values is represented by the dashed bars which indicate the lower and upper boundaries of the 95 % confidence interval (CI) of the fitting model (see Sect. 2.4 for details).

TCD
8, 4033–4074, 2014

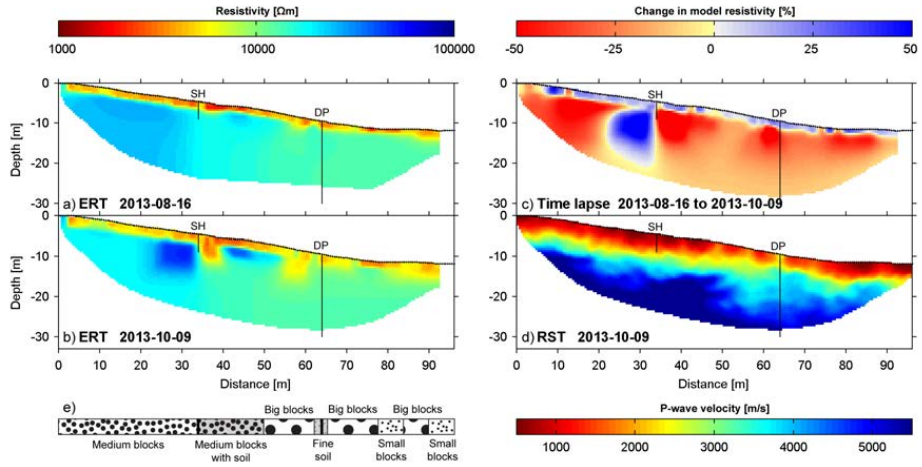

Figure 7. Tomograms of the specific resistivities for both ERT measurements: **(a)** 16 August 2013 and **(b)** 9 October 2013, **(c)** percentage change in model resistivity between the two dates and **(d)** seismic velocities. The location of SH and DP is figured with vertical black lines of respective length. A rough description of the surface aspect along the profile is also shown **(e)**.

TCD
8, 4033–4074, 2014

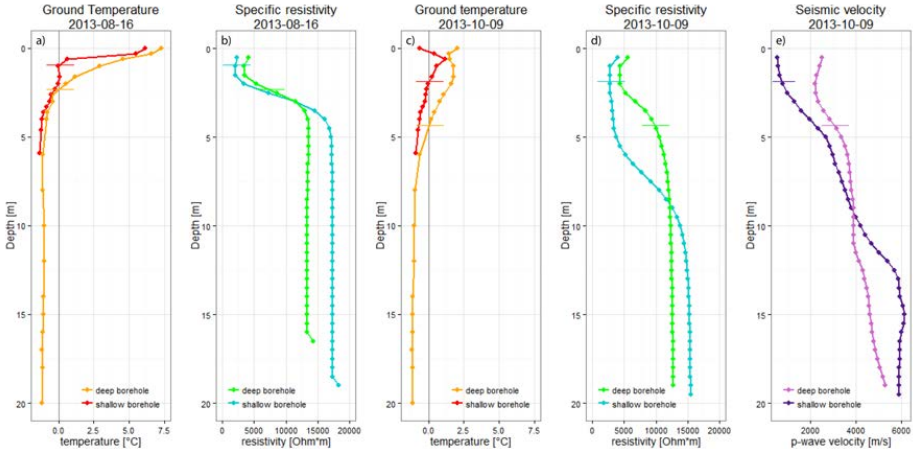

Figure 8. Vertical distribution of specific resistivity and *P* wave velocity at the borehole locations extracted from the tomograms shown in Fig. 7 as well as borehole temperatures for the dates of the ERT and RST measurements. The horizontal lines represent the active layer thickness at the respective time periods.

TCD
8, 4033–4074, 2014